Journal of South American Earth Sciences 32 (2011) 547–554

Contents lists available at ScienceDirect

Journal of South American Earth Sciences

journal homepage: www.elsevier.com/locate/jsames

The North Patagonian batholith at Paso Puyehue (Argentina-Chile). SHRIMP ages and compositional features

Eugenio Aragón [a], Antonio Castro [b,*], Juan Díaz-Alvarado [c], D.-Y. Liu [d]

[a] Centro de Investigaciones Geológicas (UNLP-CONICET), Facultad de Ciencias Naturales y Museo (UNLP) La Plata, Buenos Aires, Argentina
[b] Departamento de Geología, Universidad de Huelva, Campus del Carmen, 21071 Huelva, Spain
[c] Departamento de Geodinámica y Paleontología, Universidad de Huelva, Campus del Carmen, 21071 Huelva, Spain
[d] Beijing SHRIMP Center, Chinese Academy of Geological Sciences, Beijing, PR China

ARTICLE INFO

Article history:
Received 30 August 2010
Accepted 14 February 2011

Keywords:
Granites
U–Pb SHRIMP ages
Isotopes
Patagonia

ABSTRACT

New U–Pb SHRIMP zircon ages together with a geochemical and isotopic (Sr and Nd) study have been carried out on a hornblende gabbro, a biotite granodiorite, and host andesitic rocks of the North Patagonian batholith at Paso Puyehue, close to the Argentinean-Chilean border. The results yield ages of 18 ± 1 Ma for the gabbros and 12.4 ± 0.3 Ma for the granodiorites. An age of 125 ± 2 Ma was obtained for the host volcanic rock, and an age of 22 ± 2 Ma for the basaltic trachy-andesite. The intrusive suite is composed of dominant hornblende-biotite granodiorites and subordinate hornblende gabbros and diorites. These form a typical metaluminous calc-alkaline series. The time-isotopic magmatic evolution of plutonic and volcanic rocks shows an early Eocene beginning of disparate isotopic ratios as a consequence of coeval primitive and more crustal compositions with no spatial constraints. This disparate isotopic assemblage is also coeval with the presence of the Aluk-Farallon-SAM triple junction at this latitude and the shift of the calc-alkaline magmatism from the batholith axis to the back-arc. Considerations are made for the possibility of a Paleogene slab window by slab detachment, and the development of a new subduction front since the beginning of Nazca Plate development at the 23 Ma major ocean plate rearrangement.

1. Introduction

Combined petrological and geochronological studies of cordilleran batholiths in the Americas have shown complex evolution patterns that reveal important changes in plate tectonic and mantle dynamics during subduction at active margins (Pankhurst et al., 1992, 1999; Pankhurst and Hervé, 1994; DeCelles et al., 2009). Serious efforts with considerable advances have been made to decipher the complex evolution of the Patagonian batholith (González Díaz, 1982; Parada et al., 1987; Rapela, 1987; Rapela and Kay, 1988; Munizaga et al., 1988; Pankhurst et al., 1992, 1999; Pankhurst and Hervé, 1994; Hervé et al., 2007). However, more geochronological and geochemical data are still needed to complete a general view of its entire evolution from the Jurassic to the Miocene. The northern sector of the Patagonian batholith has been recently studied as regards geochronology and geochemistry (Castro et al., 2010, this volume) revealing new Jurassic ages in the Bariloche region.

Previous studies of the North Patagonian batholith segment (41°–47°S) show that it is a composite intrusive complex with respect to age distribution, composition and geological evolution (Castro et al., 2010, this volume; Cingolani et al., 1991; González Díaz, 1982; Munizaga et al., 1988; Pankhurst et al., 1992, 1999; Pankhurst and Hervé, 1994; Parada et al., 1987; Rapela, 1987; Rapela and Kay, 1988). The earliest records of magmatic activity at the southern segment (47°–54°S) of the North Patagonian batholith occurred in the Upper Jurassic (Hervé et al., 2007). However, north of this latitude, the earliest magmatic activity confirmed was early Cretaceous (Pankhurst et al., 1999). The Lower Cretaceous granitoids have the highest $(^{87}Sr/^{86}Sr)_i$ ratios (0.7050) and lowest ϵNd_i values (−1 to −5), with a regular and almost continuous decrease in time of the $(^{87}Sr/^{86}Sr)_i$ ratios (from 0.7045 to 0.7035) and increase of ϵNd_i values from +0.5 to +4.5. This evolution persists until Late Eocene–Oligocene, when they resume to higher values of $(^{87}Sr/^{86}Sr)_i$ ratios up to 0.7048 and lower ϵNd_i values up to +0.5. The rate of Paleogene plutonic production decreases significantly with respect to the Cretaceous and upper Miocene magmatic events. The location of the few Paleogene plutons shifts toward the core of the batholith, close to the position

* Corresponding author.
E-mail addresses: earagon@cig.museo.unlp.edu.ar (E. Aragón), dorado@uhu.es (A. Castro).

0895-9811/$ – see front matter © 2011 Elsevier Ltd. All rights reserved.
doi:10.1016/j.jsames.2011.02.005

of the large Liquiñe-Ofqui fault system (Pankhurst et al., 1999). Furthermore, as the Paleogene plutonic production is interrupted at the site of the North Patagonian batholith, a new Eocene bimodal, calc-alkaline volcanism develops at the back-arc, expressed as ignimbrite flare-up interstratified with alkali basalts (Aragón and Mazzoni, 1997; Aragón et al., 2001, 2004a,b, 2005).

Important changes in plate convergence configurations affected this sector of the Andean orogenic system during the Cenozoic (Cande and Leslie, 1986; Pardo Casas and Molnar, 1987; Somoza, 1998; Somoza and Ghidella, 2005) and, from this perspective, the orthogonal subduction stages are correlated to the productive plutonic stages of the North Patagonian batholith (Pankhurst et al., 1999).

The purpose of this study is to present the results of preliminary geochronological and geochemical research in the Paso Puyehue segment of the North Patagonian batholith, which represents the resumption of magmatic arc activity at the locus of plutonic emplacement after the Miocene major plate re-organization, and contains volcanic rocks of the synextensional Eocene–Oligocene volcanism that replaced Paleogene batholitic plutonic emplacement. The implications are most significant, in that this time may represent the inaugural moment of a new subduction front subsequent to slab detachment.

2. Geological setting

At Paso Payehue, granite intrusions are linked regionally to the northern segment of the Patagonian batholith. The country rocks are the northern-most volcanic representatives of the Divisadero Formation (Lower Cretaceous), the Western Oligocene Volcanic Belt (Rapela et al., 1987), and the volcanic–sedimentary rocks of the Ñirihuau Formation. It is difficult to define individual plutons due to the discontinuous nature of the outcrops, but one of the outcrops shows intrusive contact of a granodioritic pluton with the Divisadero Formation.

Intrusive rocks comprise granites and leucogranites. Previous K/Ar age estimates yield ranges of 43–30 Ma and 10–8 Ma for the Pireco and Tristeza granite intrusions respectively. Miocene whole rock Rb/Sr isochron and K/Ar ages ranging from 16 to 10 Ma respectively were reported for the granitoids in Chile, west of the studied area (Reloncavi granite; Parada et al., 1987). The Western Oligocene Volcanic belt (WOB) defines a typical calc-alkaline association that extends from this locality (close to the batholith, Fig. 1) to the southeast into the back-arc more than 400 km away from the plate margin (Rapela et al., 1983, 1987), under an extensional tectonic setting (Mancini and Serna, 1989; Giacosa and Heredia, 2004; Rapela et al., 1983, 1987; Silvestro and Zubiri, 2008). To the east a second and older volcanic belt is recognized in the Paleogene (Fig. 1): the Eastern Paleocene-Eocene Volcanic Belt (EPEB) (Rapela et al., 1987). Both volcanic belts contain late basalts with OIB affinity (Kay and Rapela, 1987; Aragón et al., 2005), and both are coeval with the development of the eastern and western boundaries of the Ñirihuau basin (Cazau et al., 1989; Spalletti, 1983).

Most radiometric K/Ar ages of the EPEB range from 60 to 42 Ma (Rapela et al., 1983). The EPEB is a bimodal volcanism where rhyolites and dacites predominate as large ignimbrite plateaus and subordinate domes and lava flows (Rapela et al., 1987; Aragón and Mazzoni, 1997), suggesting an ignimbrite flare-up. The WOB volcanic rocks also start as dacite-rhyolite flows and ignimbrites. The top of the sequence is mostly andesitic to basaltic, and shows a range of K/Ar radiometric ages of 24–33 Ma (Rapela et al., 1987).

In summary, important changes in plate convergence configurations have affected this sector of the Andean orogenic system during the Cenozoic (Cande and Leslie, 1986; Pardo Casas and Molnar, 1987; Somoza, 1998; Somoza and Ghidella, 2005). An important evolutionary pattern is defined by a change from low angle convergence and southward migration of the Farallon-Aluk-SAM triple junction along the northern Patagonian latitudes at the Paleogene, to the Miocene new plate reorganization due to the fracture of the Farallon

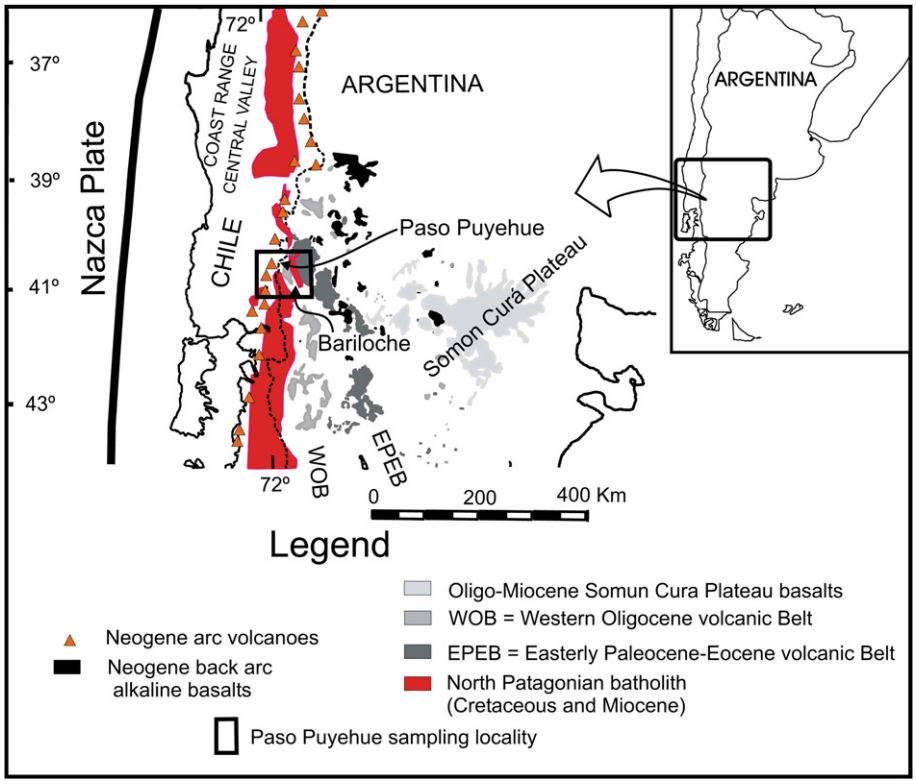

Fig. 1. Geological sketch map of the Northern Patagonia region, showing Paso Puyehue sampling locality with the distribution of the North Patagonian batholith, and the Cainozoic volcanism.

plate 23 Ma age to develop the Nazca plate (Lonsdale, 2005). The Nazca plate has subducted with almost orthogonal convergence angle with respect to the SAM plate.

3. Sampling and analytical techniques

Two samples of the intrusive rocks and two samples of volcanic country rocks were analyzed for Sr–Nd isotopes and zircon geochronology. Sample ANG2010-3 is a medium-grained hornblende gabbro (Color Index = 38). The texture is subidiomorphic and the modal mineralogy includes zoned plagioclase (An_{60-44}), hornblende and interstitial quartz (>5%). Biotite is a minor component. Main accessories are apatite, titanite, magnetite and zircon. Sample ANG2010-4 is a medium-grained biotite granodiorite (Colour Index = 7) that contain fine-grained facies of the biotite granodiorite as enclaves within the dominant and homogeneous mass of medium-grained facies. K-feldspar often develops perthitic texture. Quartz is interstitial to granular and the plagioclase is zoned oligoclase (average An_{19}). Biotite is usually chloritized, and feldspar may show local transformation to muscovite. Main accessories are apatite, magnetite, zircon and titanite. Sample ANG2010-5 is a felsitic dacite with few microphyric plagioclase and quartz filled vesicles. Groundmass has chloritized biotite. Sample ANG2010-6 is a basaltic trachy-andesite with fine pilotaxitic texture groundmass with chloritized mafic microlites. It is microphyric with zoned poikilitic plagioclase and chloritized mafic minerals. These two samples are considered as representative of the calc-alkaline volcanic successions that host the Cenozoic intrusions in this sector of the North Patagonian batholith. Sample (ANG2010-5) was collected close to the intrusive contact and, consequently, it shows signs of alteration. For that reason it was only subjected to zircon separation (no major, trace or isotopic analyses were performed).

Major elements and Zr were analyzed by X-ray fluorescence (XRF) at the University of Oviedo (Spain) using glass beads. Precision of the XRF technique was better than ±1.5% relative. Trace element and rare earth elements (REE) were analyzed by inductively coupled plasma mass spectrometry (ICP-MS) with an HP-4500 system at the University of Huelva, following digestion in an HF + HNO_3 (8:3) solution, drying and second dissolution in 3 ml HNO_3. The average precision and accuracy for most of the elements were controlled by repeated analyses of SARM-1 (granite) and SARM-4 (norite) international rock standards. They fall in the range of 5–10% relative.

Samples ANG2010-3, -4 and -6 were selected for isotopic analyses. Rb–Sr and Sm–Nd isotopic ratios were determined with a Finnigan MAT-262 mass spectrometer at the University of Granada. Samples for Sr and Nd isotope analyses were digested using ultraclean reagents and analyzed by thermal ionization mass spectrometry (TIMS) in a Finnigan Mat-262 mass spectrometer after chromatographic separation with ion-exchange resins. Normalization values were $^{86}Sr/^{88}Sr = 0.1194$ and $^{146}Nd/^{144}Nd = 0.7219$. Blanks were 0.6 and 0.09 ng for Sr and Nd, respectively. The external precision (2σ), estimated by analyzing 10 replicates of the standard WS-E (Govindaraju et al., 1994), was better than ±0.003% for $^{87}Sr/^{86}Sr$ and ±0.0015% for $^{143}Nd/^{144}Nd$. $^{87}Sr/^{86}Rb$ and $^{143}Sm/^{144}Nd$ were directly determined by ICP-MS following the method developed by Montero and Bea (1998), with a precision better than ±1.2% and ±0.9% (2σ) respectively. Nd isotopic ratios were corrected for mass fractionation using a $^{146}Nd/^{144}Nd$ ratio of 0.7219.

Zircon separation was accomplished by traditional techniques using dense liquids and magnetic (Frantz) separation. Selected crystals free of impurities and fractures were selected by hand-picking with a binocular lens. These were mounted in epoxy, together with reference standards, 91500 and TEMORA, and polished. Sectioned zircons were studied by CL imaging for selection of point analyses. Core and rims were analyzed in several grains of each

Table 1
Whole rock analyses of major and trace elements and Sr–Nd isotopes of Paso Puyehue samples.

Sample	ANG2010-3	ANG2010-4	ANG2010-6
Lat.	S40° 44.221	S40° 44.848	S40° 44.868
Long.	W71° 53.618	W71° 51.022	W71° 50.895
Rock type	Gabbro	Granodiorite	Andesite
wt.%			
SiO_2	52.44	68.84	52.37
TiO_2	0.85	0.41	1.49
Al_2O_3	17.01	16.72	18.91
FeOt	7.42	2.06	8.68
MgO	5.83	0.49	3.45
MnO	0.19	0.09	0.32
CaO	10.72	2.04	5.42
Na_2O	2.44	5.12	4.72
K_2O	0.4	2.74	2.08
P_2O_5	0.15	0.10	0.52
Loi	0.64	0.26	0.37
Total	98.10	98.87	98.33
Mg#[a]	0.58	0.30	0.41
ASI[b]	0.72	1.12	0.98
ppm			
Li	2.78	7.58	26.8
Be	0.54	1.20	1.94
Sc	34.2	2.84	28.8
V	209	7.89	155
Cr	104	8.45	17.4
Co	36.9	27.6	20.5
Ni	61.6	13.5	6.13
Cu	56.6	1.89	5.18
Zn	61.5	23.4	235
Ga	14.6	16.1	27.3
Rb	5.97	60.5	64.9
Sr	332	294	196
Y	16.6	15.4	40.2
Zr[c]	82.8	312	139
Nb	3.30	7.95	4.39
Cs	0.20	1.39	2.95
Ba	91.3	785	831
La	9.03	52.9	15.9
Ce	18.5	97.8	37.4
Pr	2.44	10.8	5.33
Nd	10.7	39.9	25.7
Sm	2.74	6.14	6.53
Eu	0.93	1.80	2.19
Gd	2.93	4.55	6.89
Tb	0.50	0.58	1.12
Dy	2.99	3.26	6.86
Ho	0.62	0.58	1.42
Er	1.71	1.42	3.86
Tm	0.27	0.20	0.58
Yb	1.62	1.18	3.44
Lu	0.24	0.17	0.48
Hf	1.20	0.20	0.99
Ta	1.29	2.35	0.63
Pb	2.68	10	11.8
Th	2.10	12.3	2.03
U	0.52	1.17	0.36
Rb	5.97	60.5	64.9
Sr	332	294	196
$^{87}Rb/^{86}Sr$	0.052	0.595	0.957
$^{87}Sr/^{86}Sr$	0.70355	0.70377	0.70456
2SD (%)	0.002	0.002	0.002
$(^{87}Sr/^{86}Sr)$ t	0.7035	0.7037	0.7042
Sm	2.74	6.14	6.53
Nd	10.7	39.9	25.6
$^{147}Sm/^{144}Nd$	0.1541	0.0929	0.154
$^{143}Nd/^{144}Nd$	0.51292	0.51287	0.51282
2SD (%)	0.003	0.002	0.002
$(^{143}Nd/^{144}Nd)$ t	0.51290	0.51287	0.51280
εNd	5.6	4.8	3.7
T DM (Ga)	0.366	0.424	0.515

[a] Mg# = Mol MgO/(MgO + FeOT).
[b] ASI = Mol $Al_2O_3/(CaO + Na_2O + K_2O)$.
[c] XRF analyses (the rest are ICP-MS determinations).

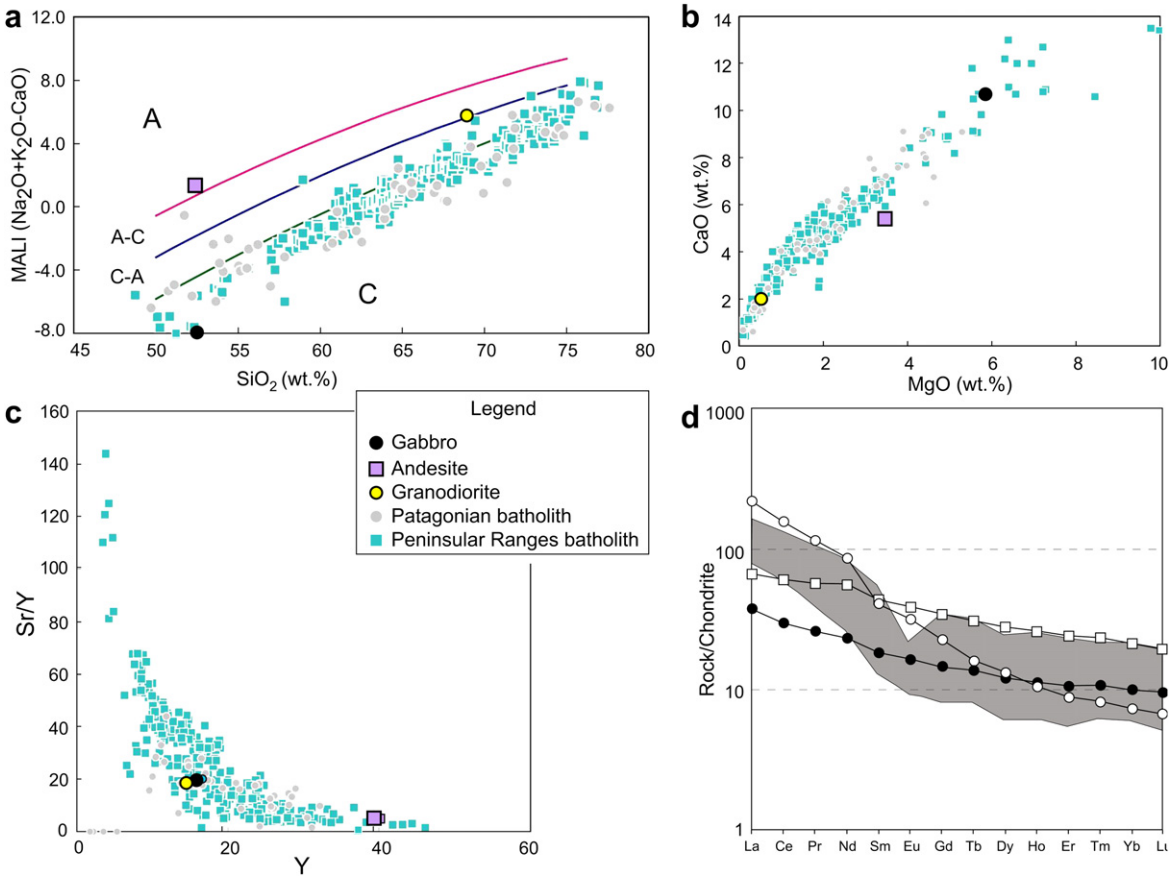

Fig. 2. Geochemical diagrams showing relevant geochemical variations of samples from Paso Puyehue. Samples from the Patagonian batholith (Hervé et al., 2007; Pankhurst et al., 1999) and the Peninsular Ranges batholith in North America (Lee et al., 2006) are shown in the background for comparisons. (a) MALI-silica diagram (Frost et al., 2001) A = Alkalic, A-C = Alkalic-Calcic, C-A = Calcic-Alkalic, and C=Calcic. (b) CaO vs. MgO and (c) Sr/Y vs. Y diagrams. (d) Chondrite normalized (Nakamura, 1974) REE diagram. Grey field; Granites from the Bariloche area, (Castro et al., 2010, this volume) are taken as a reference in the diagram.

individual sample with the aim of identifying inherited cores. These selected points were targeted over the CL images and analyzed for U–Th–Pb isotopes with SHRIMP II at the Beijing-SHRIMP Center (Chinese Academy of Geological Sciences, Beijing), following methods given in Williams (1998) and references therein. The data were processed with ISOPLOT software for Concordia plots, probability density plots, stacked histograms and weighted means and Concordia age calculations.

4. Geochemical features

Analytical data of the studied samples are listed in Table 1. These samples are representative of the main plutonic rocks that form Cenozoic intrusions at the north end of the Patagonian batholith. The granitoid is a typical cordilleran, low-K granodiorite. It plots among the granodiorite and tonalite fields of the Or–Ab–An classification diagram (not shown), and at the calc-alkaline trend in all major element diagrams (e.g. CaO–MgO in Fig. 2). Only the Na_2O content is higher than normal compared with other cordilleran batoliths, causing the sample to be plotted at the limit between calc-alkalic and alkali-calcic series in the MALI-silica diagram (Fig. 2). Trace elements are also characteristic of cordilleran calc-alkaline granitoids, with moderate REE fractionation (CeN/YbN = 30.5) and moderate Sr/Y ratios of 19.1.

The hornblende gabbro belongs to a calcic series in the MALI-silica diagram. It also shows major elements and Sr, Ba and REE compositions similar to the Tertiary hornblende gabbros and diorites of the Cayute Unit (Parada et al., 1987) of the cordilleran calc-alkaline granitoids at the western side of the Andes and at the same latitude of the sampled area in this study.

The Oligocene volcanic rock shows notorious differences with respect to present day volcanic arc rocks at this latitude. It is a basaltic trachy-andesite with a Na_2O content higher than normal calc-alkaline andesites. The high alkali content of this rock causes to be plotted at the Alkalic series in the MALI-silica diagram (Fig. 2), nevertheless, a small amount of normative hypersthene is present, showing the transitional nature of this rock. It is extremely enriched in K_2O, Na_2O, TiO_2, P_2O_5, Rb, Ba and REE and impoverished in Mg_2O, CaO and Sr compared to basalts (with similar SiO_2 values from Tormey et al., 1991) erupted along the current volcanic arc front at the same latitude.

The isotopic composition of the sampled Miocene granitoids is characterized by low $^{87}Sr/^{86}Sr$ initial ratios (0.7037) and positive values of $\epsilon Nd = +4.8$. These primitive features are shared by the sampled Hbl gabbro, which has $^{87}Sr/^{86}Sr = 0.7035$ and $\epsilon Nd = +5.6$. The Upper Oligocene basaltic trachy-andesite has initial $^{87}Sr/^{86}Sr = 0.7042$ and $\epsilon Nd = +3.7$ (Table 1).

5. Zircon geochronology

Zircon grains in samples ANG2010-3 and ANG2010-4 are large euhedral, elongated crystals with typical igneous parallel banding, and a minor amount of small prismatic zircon crystals with concentric oscillatory zoning. Analyses provide a weighted $^{206}Pb–^{238}U$ mean age of 18 ± 1 Ma (MSWD = 2.9) and 12.4 ± 0.3 Ma (MSWD = 0.89) for samples ANG2010-3 and ANG2010-4

respectively (Fig. 3a and b, Table 2). Zircon crystals in sample ANG2010-5 are euhedral crystal with continuous concentric overgrowths (Fig. 3c). Six point analyses give a weighted $^{206}Pb–^{238}U$ mean age of 125 ± 2 Ma (MSWD = 1.5). A younger age of 17.2 Ma must be related to fine veins of the granodiorite (ANG2010-4) intrusion. In sample ANG2010-6, zircon grains are small prismatic crystals without concentric overgrowths (Fig. 3d). Measured $^{206}Pb/^{238}U$ ages are around 22 Ma and only one of the analyses gives an age older than 25 Ma (Table 2). A Tera-Wasserburg Concordia diagram (Fig. 3d) was used for this sample resulting and 3 younger analyses provide a weighted mean $^{206}Pb/^{238}U$ age of 22 ± 2 Ma.

All samples are lack of inherited cores.

6. Final remarks and discussion

The most relevant geological improvements that the new U–Pb SHRIMP, geochemical and isotopic data presented in this paper are defined below.

6.1. The U–Pb SHRIMP data

The new U–Pb SHRIMP data show: (1) Sample (Ang2010-5) is the northernmost volcanic Lower Cretaceous locality that can be correlated to Divisadero Formation. (2) Sample (Ang2010-6), the (transitional) basaltic trachy-andesite, corroborates the presence of Lower Miocene–Upper Oligocene volcanic activity of the WOB at the locus of the North Patagonian batholith, at the time that there is a plutonic emplacement gap, and the calc-alkaline volcanic activity (with basalts of OIB affinity) spreads from the fore-arc to the back-arc (Muñoz et al., 2000; Kay and Rapela, 1987). (3) Sample (Ang2010-3) is the first known Tertiary gabbro on the Argentinian side of the North Patagonian batholith, and can be correlated to the Cayute and Peninsula Rollizos gabbros (Parada et al., 1987) at the western side of the Andes. It is also the first U–Pb age that confirms the Lower Miocene emplacement of the gabbros at the reinstatement of plutonic activity at the locus of the North Patagonian batholith after the Oligocene gap. (4) Sample (Ang2010-4) 12 Ma age, suggests that the more evolved quartz-monzodiorites,

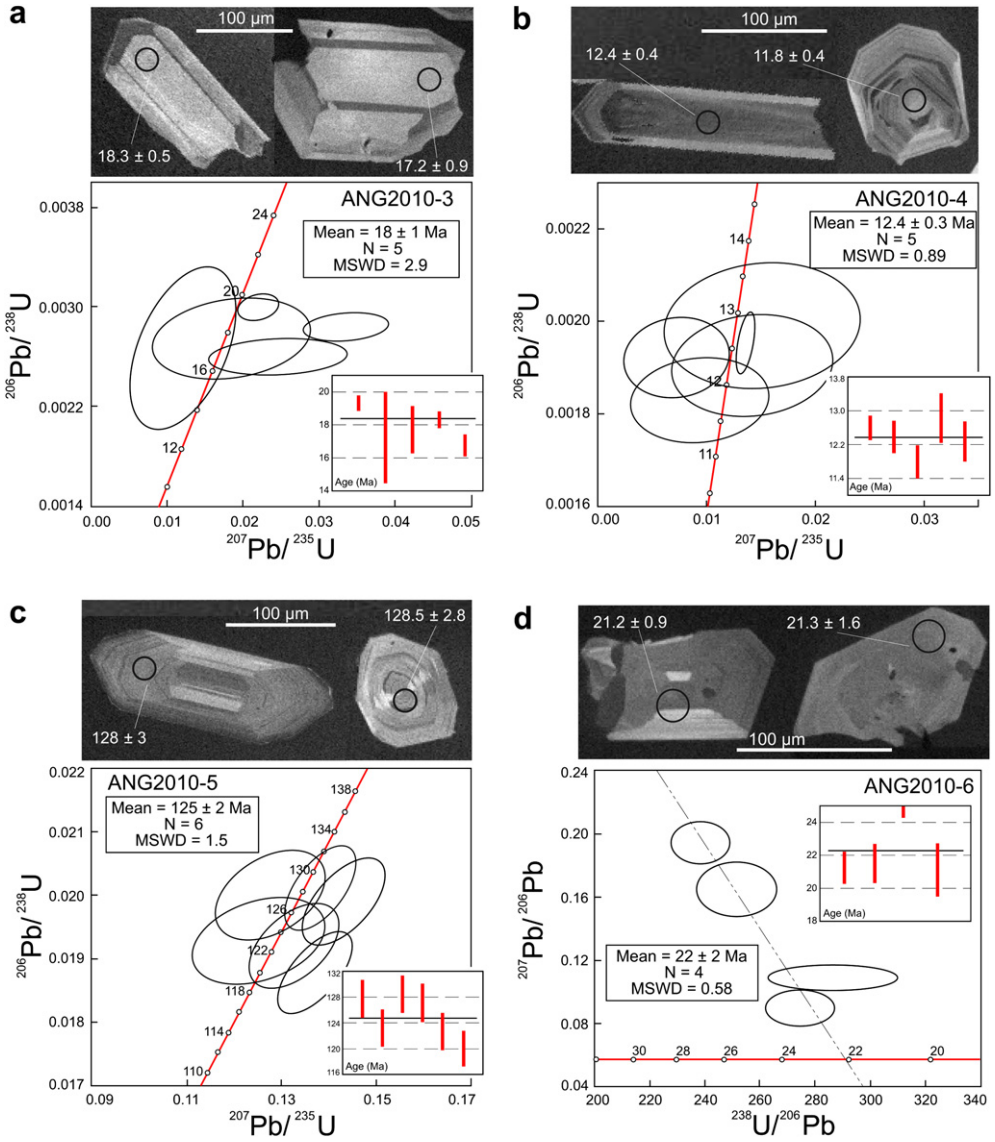

Fig. 3. (a–c) Concordia plots of SHRIMP U–Pb isotopic analyses for samples ANG2010-3 to -5 from Paso Puyehue. Plots include 2σ error bars diagrams. (d) Tera-Wasserburg Concordia diagram for sample ANG2010-6. Data-point error ellipses are 68.3% conf. Concordia plots include insets with weighted $^{206}Pb–^{238}U$ mean ages (95% conf.) and statistical information 1σ error bars diagrams are included too. Cathodoluminescence images of representative zircon crystals are shown above each Concordia plot.

Table 2
Summary of SHRIMP U–Pb zircon data for Paso Puyehue samples.

Grain and spot	^{206}Pb (ppm)	^{206}Pbc %	^{238}U (ppm)	^{232}Th (ppm)	Th/U	^{206}Pb/^{238}U	± %	^{238}U/^{206}Pb	± %	^{207}Pb/^{235}U	± %	^{207}Pb/^{206}Pb	± %	^{206}Pb/^{238}U age (Ma)	±
Sample ANG2010-3 (diorite)															
1,1	1.67	0.64	645	731	1.17	0.00300	2.3	331	2.3	0.0221	8.0	0.0535	7.6	19.3	0.5
2,1	1.63	4.04	683	1077	1.63	0.00267	16	359.1	16.1	0.0122	38	0.033	34	17.2	2.8
3,1	0.49	6.27	193	57	0.30	0.00275	7.9	340.6	7.7	0.0184	37	0.049	36	17.7	1.4
4,1	0.76	0.00	311	211	0.70	0.00284	2.6	351.6	2.6	0.0335	11	0.0855	11	18.3	0.5
5,1	0.51	13.69	192	109	0.59	0.00267	5.1	323.7	3					17.2	0.9
6,1	0.50	4.29	216	181	0.87	0.00260	3.8	367.7	3.7	0.0247	24	0.069	24	16.8	0.6
7,1	0.16	16.39	52	19	0.38	0.00290	14	287.8	4.6					18.7	2.6
Sample ANG2010-4 (granodiorite)															
1,1	5.06	0.20	3003	6779	2.33	0.00196	2.2	510.3	2.2	0.0137	4.2	0.0508	3.5	12.6	0.3
2,1	1.47	3.52	859	957	1.15	0.00192	3.0	501.7	2.7	0.0074	43	0.028	43	12.4	0.4
3,1	1.10	5.72	659	423	0.66	0.00183	3.3	515	2.7	0.0095	44	0.038	44	11.8	0.4
4,1	0.69	8.29	430	260	0.62	0.00172	4.4	534.2	3.1					11.1	0.5
5,1	0.34	7.14	183	170	0.96	0.00199	4.5	466	3.8	0.0152	39	0.055	39	12.8	0.6
6,1	0.56	5.29	326	343	1.09	0.00191	3.8	497	3.1	0.0142	34	0.054	34	12.3	0.5
Sample ANG2010-5 (dacite)															
1,1	4.58	0.79	264	167	0.65	0.02001	2.3	49.6	2.3	0.1278	6.0	0.0463	5.5	127.7	2.9
2,1	0.76	0.99	328	222	0.70	0.00267	3.0	370.3	3.0	0.0235	11	0.0637	11	17.2	0.5
3,1	4.90	0.89	293	198	0.70	0.01930	2.3	51.4	2.3	0.1254	7.4	0.0471	7.0	123.2	2.8
4,1	8.84	0.14	511	469	0.95	0.02013	2.2	49.6	2.2	0.1383	3.6	0.0499	2.8	128.5	2.8
5,1	5.03	0.21	293	191	0.67	0.01992	2.3	50.1	2.3	0.1432	3.9	0.0522	3.2	127.1	2.9
6,1	4.48	0.22	271	210	0.80	0.01921	2.3	52	2.3	0.1328	4.7	0.0501	4.1	122.7	2.8
7,1	5.75	0.13	356	214	0.62	0.01879	2.3	53.1	2.3	0.1372	3.7	0.0529	2.9	120.0	2.7
Sample ANG2010-6 (andesite)															
1,1	0.87	9.32	277	372	1.39	0.00329	4.5	274.7	3.0			0.0900	8.3	21.2	0.9
2,1	0.98	4.37	327	393	1.24	0.00333	5.7	287	5.4	0.0341	21.3	0.1087	4.7	21.4	1.2
3,1	0.70	4.00	195	168	0.89	0.00402	3.0	238.5	3.0	0.0925	6.2	0.1946	4.4	25.9	0.8
4,1	0.33	16.93	97	80	0.85	0.00328	7.9	251.6	3.8			0.1640	6.8	21.1	1.7

Errors are 1-σ, Pb_c = common Pb. Common Pb corrected using measured ^{206}Pb in all isotopic ratios and ages.

tonalites, granodiorites and leucogranites are younger than the gabbros at this locality, and corroborates an Upper Miocene age for this suite at the eastern side of the Andes.

6.2. The age constrained isotopic data and the tectono-magmatic setting

The new age constrained isotopic data is consistent with the previous published data (Pankhurst et al., 1999). The notorious time-dependent isotopic evolution of Patagonia active margin magmatism (Fig. 4, modified from Pankhurst et al., 1999) shows three major stages in terms of their isotopic composition and tectono-magmatic setting: The first stage shows that the North Patagonian batholith has evolved from crustal magmas in the early Cretaceous, to more primitive magmas in the early Paleocene (Pankhurst et al., 1999; Hervé et al., 2007), and coincides with the Aluk plate subduction. The second stage (Eocene–early Miocene) shows a disparate isotopic assemblage of primitive along with more crustal magmas, plutonic emplacement at the batholith decreases to extinction, the Eocene calc-alkaline magmatic locus (synextensional) migrates eastward to the back-arc (Fig. 1), and the Oligocene–early Miocene calc-alkaline magmatic locus (synextensional) spreads all through fore-arc, arc and back-arc, with the distinct fact that Eocene to early Miocene basalts show OIB signatures (Muñoz et al., 2000; Kay and Rapela, 1987). This stage coincides closely with the moment when the Paleocene clockwise-rotating Farallon-Aluk active spreading Ridge reaches SAM at the Latitude of Patagonia to establish the Farallon-Aluk-SAM triple junction (Cande and Leslie, 1986). The third stage shows that the magmatic locus has returned to the North Patagonian batholith (late Miocene) with relatively larger amounts of gabbros, and is evolving to more primitive magmas towards the recent SVZ. The beginning of this stage starts following the Farallon plate-splitting at 23 Ma (Lonsdale, 2005) and the development of Nazca plate.

6.3. The calc-alkaline magmatic locus shift

Pankhurst et al. (1999) showed that the periods of granitoid emplacement in the North Patagonian batholith have coincided closely with periods of rapid orthogonal convergence but, instead, the Eocene–Lower Miocene stage shows a calc-alkaline magmatic locus shift to the back-arc (Aragón et al., 2008). This stage coincides with a plate triple junction, low plate convergence angles (Cande and Leslie, 1986; Pardo Casas and Molnar, 1987; Somoza and Ghidella, 2005) and, although much uncertainty exists regarding the subduction rates for this latitude (Pardo Casas and Molnar, 1987), negative to null convergence rates are registered at 40°S during the 60–50 Ma period as the plates R-T-T (active Ridge-Trench-Trench) triple junction existed at this latitude. The trace element OIB affinity of the basalts of this stage suggest an Eocene and Oligocene slab window (Espinoza et al., 2005; Muñoz et al., 2000), this is reinforced by the synextensional character of this volcanism. The main end case hypotheses suggested to explain this slab window event are; slab roll-back (Muñoz et al., 2000) and slab detachment (Aragón et al., 2008). In this respect, the early Eocene beginning of the disparate isotopic assemblage of primitive along with more crustal compositions for the synextensional widespread magmatism of this stage, as confirmed by the EPEB ignimbrite flare-up isotopic compositions (Fig. 4) (Castro and Aragón unpublished data), and the negative to null convergence rate for the 50–60 Ma span at this latitude, rules out slab roll-back. Instead the presence of an R-T-T triple junction and the highly oblique plate convergence suggest that the large slab window may be caused by a slab detachment. If this is so, then the major Miocene plate rearrangements (23 Ma), along with the onset of the orthogonal subduction of the Nazca plate, should be considered as a new subduction front at this particular segment of the Andes, and could explain the return of the magmatic locus to the North Patagonian batholith, with the unusual abundance of

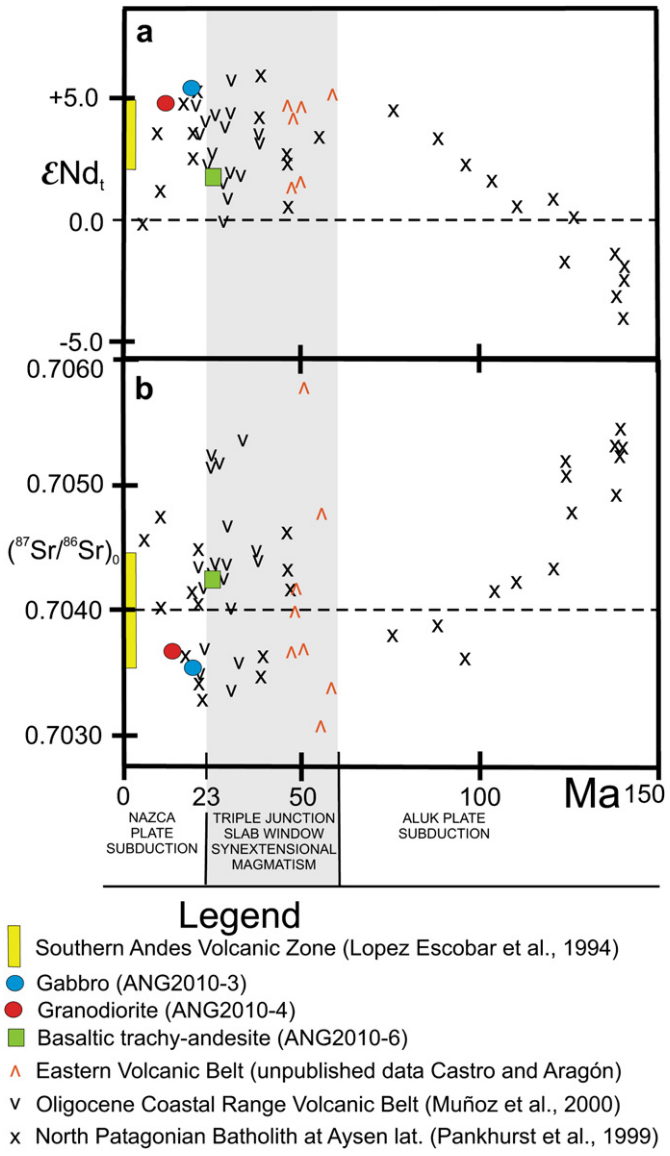

Fig. 4. (a) εNd_t and (b) Initial $^{87}Sr/^{86}Sr$ ratio vs. crystallization age for North Patagonian batholith granitoids and Paleogene volcanism, modified from Pankhurst et al. (1999). X; North Patagonian batholith at Aysen (Pankhurst et al., 1999): V; Coastal Range Oligocene volcanic belt (Muñoz et al., 2000): Red circle; basaltic trachy-andesite (this paper): Red square; Granitoids (this Paper): Orange inverted V; volcanic rocks from the Eastern Paleocene–Eocene volcanic belt EPEB (Castro and Aragón unpublished data): Yellow rectangle: Southern Andes Volcanic zone SVZ (López-Escobar et al., 1995): The grey shaded field shown is for the Aluk-Farallon-SAM triple junction stage at this Latitude, and the slab window event suggested from Paleogene western coast volcanic rocks geochemistry (Muñoz et al., 2000; Espinoza et al., 2005) and this paper. Farallon plate-splitting and Nazca plate-spreading beginning is placed at 23 Ma after Lonsdale (2005). (For interpretation of the references to colour in this figure legend, the reader is referred to the web version of this article.)

early gabbros that in this study show a U–Pb SHRIMP age of 18 ± 1 Ma.

Acknowledgements

We grately appreciate the help of M. Woodburne and E. Llambias. Sampling, petrology and SHRIMP studies were funded with research grants from the Spanish Ministry of Science and Innovation (Projects CGL2007-63237/BTE). Field-work was supported to E. Aragón with grants from projects of UNLP 11N/534, CONICET PID 00916 and PRIN-COFIN 2007.

References

Aragón, E., Mazzoni, M.M., 1997. Geología y estratigrafía del complejo volcánico piroclástico del río Chubut medio (Eoceno), Chubut, Argentina. Revista de la Asociación Geológica Argentina 52 (3), 243–256.

Aragón, E., Aguilera, Y., González, P., Gómez Peral, L., Cavarozzi, C.E., 2001. El Intrusivo Florentina del Complejo Volcánico Piroclástico del Río Chubut medio: un ejemplo de Etmolito o Embudo. Revista de la Asociación Geológica Argentina 56 (2), 161–172.

Aragón, E., González, P., Aguilera, Y., Marquetti, C., Cavarozzi, C.E., Ribot, A., 2004a. El domo vitrofírico Escuela Piedra Parada del Complejo volcánico piroclástico del río Chubut Medio. Revista de la Asociación Geológica Argentina 59 (4), 607–618 (Patagonia Special Issue).

Aragón, E., Aguilera, Y., Consoli, V., Cavarozzi, C.E., Ribot, A., 2004b. Las Andesitas Estrechura del Complejo Volcánico Piroclástico del Río Chubut medio (Paleoceno-Eceno medio). Revista de la Asociación Geológica Argentina 59 (4), 619–633 (Patagonia Special Issue).

Aragón E., Aguilera Y., Cavarozzi C., Ribot A., 2005. Basaltos Alcalinos en el Complejo Volcánico-Piroclastico del Río Chubut medio. In: Actas XVI Congreso Geologico Argentino. Actas 1, pp. 485–486.

Aragón, E., Aguilera, Y., Cavarozzi, C.E., Ubaldon, M.C., Ribot, A., 2008. La Caldera de Piedra Parada. Un volcán gigante de 50 millones de años, testimonio de cambios. In: Ardolino, A., CSIGA (Eds.), Sitios de Interés Geológico, Tomo 2. Servicio Geológico Minero Argentino, pp. 669–682.

Cande, S.C., Leslie, R.B., 1986. Late Cenozoic tectonics of the Southern Chile trench. Journal of Geophysical Research 91 (B1), 471–496.

Castro, A., Moreno-Ventas, I., Fernández, C., Vujovich, G., Gallastegui, G., Heredia, N., Martino, R. D., Becchio, R., Corretgé, L. G., Díaz-Alvarado, J., Such, P., García-Arias, M., Liu, D.-Y. Petrology and SHRIMP U-Pb zircon geochronology of Cordilleran granitoids of the Bariloche area, Argentina. Journal of South American Earth Sciences (this volume).

Castro, A., Geyra, T., García-Casco, A., Fernández, C., Díaz Alvarado, J., Moreno-Ventas, I., Loew, I., 2010. Melting relations of MORB-sediment mélanges in underplated mantle wedge plumes. Implications for the origin of cordilleran-type batholiths. Journal of Petrology 51, 1267–1295.

Cazau, L., Mancini, D., Cangini, J., Spallettil, L., 1989. Cuenca Ñirihuau. In: Chebli, G., Spalletti, L. (Eds.), Cuencas Sedimentarias de Argentina, Correlación Geológica, vol. 6, pp. 299–318.

Cingolani, C., Hervé, F., Munizaga, F., Pankhurst, R.J., Parada, M.A., Rapela, C., 1991. The magmatic evolution of Northern Patagonia; New impressions of pre-Andean and Andean Tectonics. Geological Society of America Special Paper 265, 29–44.

DeCelles, P.G., Ducea, M., Kapp, P., Zandt, G., 2009. Cyclicity in Cordilleran orogenic systems. Nature Geoscience 2, 251–257.

Espinoza, F., Morata, D., Pelleter, E., Maury, R.C., Suárez, M., Lagabriele, Y., Polvé, M., Bellon, H., Cotten, J., De la Cruz, R., Guivel, C., 2005. Petrogenesis of the Eocene and Mio-Pliocene alkaline basaltic magmatism in Meseta Chile Chico, southern Patagonia, Chile: evidence for the participation of two slab windows. Lithos 82, 315–343.

Frost, B.R., Barnes, C.G., Collins, W.J., Arculus, R.J., Ellis, D.J., Frost, C.D., 2001. A geochemical classification for granitic rocks. Journal of Petrology 42, 2033–2048.

Giacosa, R., Heredia, N., 2004. Structure of the north Patagonian thick-skinned fold-and-thrust belt, southern Central Andes, Argentina (41°–42° S). Journal of South American Earth Sciences 18, 61–72.

González Diaz, E.F., 1982. Geocronological zonation of granitic plutonism in the northern Patagonian Andes of Argentina: the migration of intrusive cycles. Earth Science Review 18 (3–4), 365–393.

Govindaraju, K., Potts, P.J., Webb, P.C., Watson, J.S., 1994. Report on Whin sill dolerite WS-S from England and Pitscurrie microgabbro PM-S from Scotland: assessment by one hundred and four international laboratories. Geostandard Newsletters 18, 211–300.

Hervé, F., Pankhurst, R.J., Fanning, C.M., Calderón, M., Yaxley, G.M., 2007. The South Patagonian Batholith: 150 My of granite magmatism on a plate margin. Lithos, 373–394.

Kay, S.M., Rapela, C.W., 1987. El volcanismo del Terciario inferior y medio en los Andes Norpatagónicos (40°–42° 30'S): Origen de los magmas y su relación con variaciones en la oblicuidad de la zona de subducción. In: 10° Congreso Geológico Argentino, Actas, vol. 4, pp. 192–194.

Lee, C.T.A., Cheng, X., Horodyskyj, U., 2006. The development and refinement of continental arcs by primary basaltic magmatism, garnet pyroxenite accumulation, basaltic recharge and delamination: insights from the Sierra Nevada, California. Contributions to Mineralogy and Petrology 151, 222–242.

Lonsdale, P., 2005. Creation of the Cocos and Nazca plates by fission of the Farallón plate. Tectonophysics 404, 237–264.

López-Escobar, L., Cembrano, J., Moreno, H., 1995. Geochemistry and tectonics of the Chilean Southern Andes basaltic Quaternary volcanism (37°–46°S). Revista Geológica de Chile 22 (2), 219–234.

Mancini, C.D., Serna, M.J., 1989. Evaluación petrolera de la cuenca de Ñirihuau, Sudoeste de la Argentina. In: I Congreso Nacional de Hidrocarburos, vol. 2, pp. 739–762.

Montero, P., Bea, F., 1998. Accurate determination of 87Sr/86Sr and 143Sm/144Nd ratios by inductively coupled-plasma mass spectrometry in isotope geosciences: an alternative to isotope dilution analysis. Analytica Chemica Acta 358, 227–233.

Munizaga, F., Hervé, F., Drake, R., Pankhurst, R., Brook, M., Snelling, N., 1988. Geochronology of the granitoids of the Andean lake region 39a–42aLat. South Central Chile, preliminary results. Journal of South American Earth Sciences 1, 309–316.

Muñoz, J., Troncoso, R., Duhart, P., Crignola, P., Farmer, L., Stern, C.R., 2000. The Mid-tertiary coastal magmatic belt in south-central Chile (36°–43°S): it's relation to crustal extension, mantle upwelling, and the late Oligocene increase in the rate of oceanic plate subduction beneath South America. Revista Geológica de Chile 27 (2), 177–203.

Nakamura, N., 1974. Determination of REE, Ba, Fe, Mg, Na and K in carbonaceous and ordinary chondrites. Geochimica et Cosmochimica Acta 38 (5), 757–775.

Pankhurst, R.J., Hervé, F., 1994. Granitoid age distribution and emplacement control in the North Patagonian batholith, Aysén, Southern Chile. In: 7° Congreso Geológico Chileno, Concepción, Actas, vol. 2, pp. 1409–1413.

Pankhurst, R.J., Hervé, F., Rojas, L., Cembrano, J., 1992. Magmatism and tectonics in continental Chiloé (42°–42°30′S). Tectonophysics 205, 283–294.

Pankhurst, R.J., Weaver, S.D., Hervé, F., Larrondo, P., 1999. Mesozoic-Cenozoic evolution of the North Patagonian Batholith in Aysén, Southern Chile. Journal of the Geological Society, London 156, 673–694.

Parada, M.A., Godoy, E., Hervé, F., Thiele, R., 1987. Miocene calc-alkaline plutonism in the Chilean Southern Andes. Revista Brasileira de Geociencias 17 (4), 450–455.

Pardo Casas, F., Molnar, P., 1987. Relative motion of the Nazca (Farallon) and South American plates since late Cretaceous time. Tectonics 6 (3), 233–248.

Rapela, C.W., Kay, S.M., 1988. Late Paleozoic to recent magmatic evolution of Northern Patagonia. Episodes 11 (3), 176–182.

Rapela, C.W., Spalletti, L., Merodio, J.C., 1983. Evolución magmática y geotectónica de la Serie Andesitica andina (Paleoceno-Eoceno) en la cordillera norpatagónica. Revista de la Asociación Geológica Argentina 38 (3–4), 469–484.

Rapela, C.W., Spalletti, l, Merodio, J.C., Aragón, E., 1987. Temporal evolution and spatial variation of the lower Tertiary Andean volcanism (40–42 30′S). Journal of South American Earth Sciences 1, 1–14.

Rapela, C.W., 1987. El Batolito Patagónico entre 40°30′ y 41°15′S; Estudio Geoquímico preliminar. In: Actas del X Congreso Geológica Argentino, Tucumán, Argentina, vol. 4, pp. 21–23.

Silvestro, J., Zubiri, M., 2008. Convergencia oblicua: Modelo estructural alternativo para la dorsal Neuquina (39°S)- Neuquén. Revista de la Asociación Geológica Argentina 63 (1), 49–64.

Somoza, R., Ghidella, M.E., 2005. Convergencia en el margen occidental de América del Sur durante el Cenozoico: subducción de las placas de Nazca, Farallón y Aluk. Revista de la Asociación Geológica Argentina 60 (4), 797–809.

Somoza, R., 1998. Updated Nazca (Farallón)-South America relative motions during the last 40 Ma: implications for mountain building in the Central Andean region. Journal of South American Earth Sciences 11, 211–215.

Spalletti, L.A., 1983. Paleogeografía de la Formación Ñirihuau y sus equivalentes en la región occidental de Neuquén, Río Negro y Chubut. Revista de la Asociación Geológica Argentina 38 (3–4), 454–468.

Tormey, D.R., Hykey-Vargas, R., Frey, F.A., López Escobar, L., 1991. Recent lavas from the Andean volcanic front (33 to 42°S); Interpretations of along-arc compositional variations. Geological Society of America Special Paper 265, 57–77.

Williams, L.S., 1998. U-Th-Pb geochronology by ion microprobe. In: McKibben, M.A., Shanks, W.C., Ridley, W.L. (Eds.), Applications of Microanalytical Techniques to Understanding Mineralizing Processes. Reviews in Economic Geology vol. 7, pp. 1-35